Novel wavelet threshold multi-point method for smoothing low-count gamma spectra*

Xi-Yu Yang,[1] Jian Shan,[1] Yi-Xin He,[1] and Hui Yang[1,†]

[1]*School of Nuclear Science and Technology, University of South China, Hengyang 421001, China*

During the measurement of low- and intermediate-level radioactive waste (LILW), various factors can obscure weak peaks in low-count gamma spectra to different extents. Hence, before the gamma spectra of LILW are analyzed, these factors should be eliminated through effective smoothing. This study aimed to address the loss of weak peak information in gamma spectra due to the low energy resolution of $LaBr_3$(Ce) detectors during smoothing. For the first time, this study integrated the discrete wavelet transform (a transform that decomposes a given signal into a number of sets), Nyquist sampling rate (the lowest sampling rate that permits accurate reconstruction of a sampled analog signal), and fast Fourier transform (an algorithm that computes the discrete Fourier transform of a sequence). Through this integration, this study established an optimal criterion for the decomposition level, an adaptive threshold correction model, and a novel threshold function tailored to smoothing low-count gamma spectra. Experimental results demonstrated that the proposed method enhances the signal-to-noise ratio of an original gamma spectrum by 2.51 times. Compared with traditional methods, the novel method substantially reduced the root mean square error between the smoothed and original spectra by 87.1%, achieving this with a lower smoothness value. Furthermore, it mitigated channel distortions in the full-width at tenth-maximum for the characteristic peaks of the low-count spectrum by 75.0% to 96.9%. Under different peak distances, the peak-to-valley ratio of the overlapping peaks smoothed by the novel method increased by up to 7.4% compared with other methods. This method removes noise efficiently, preserves the original data of low-count spectra, and optimizes the peak-to-valley ratio of overlapping peaks. The results of this research broaden the potential application scenarios of the $LaBr_3$(Ce) detector in LILW measurements, as well as in other fields, such as regional geophysical exploration, radiation environment monitoring, nuclear medicine, and astrophysical measurements. It substantially reduces the cost of establishing measurement systems for low-activity radioactive materials in complex environments.

Keywords: Low- and intermediate-level radioactive waste, Gamma spectrum analysis, Discrete wavelet transform, Smoothing, $LaBr_3$(Ce) detectors

I. INTRODUCTION

The operation and decommissioning stages of nuclear power plants are the primary sources of radioactive waste [1–3]. In particular, low- and intermediate-level radioactive waste (LILW) accounts for 70.63% of the total waste volume [4]. Before management and disposal measures for LILW are implemented, its potential hazard level should be assessed using specific characterization methods [5]. Gamma scanning is considered an effective method for precisely characterizing LILW [6–8]. Spectrum analysis accuracy, a core aspect of gamma scanning, directly affects characterization precision. However, the LILW gamma spectrum is complex and varies because of several factors. These include background radiation, Compton scattering in the low-energy region, gamma count fluctuations, and electronic noise. These factors obscure weak peaks, either partially or completely [9]. This substantially increases the difficulty of accurate radionuclide identification and extraction. To address this problem, high-resolution HPGe detectors have been widely used for LILW measurements. These detectors simplify radionuclide identification [10].

However, problems occur when using HPGe detectors for LILW measurements. The main problem is the extended measurement time, which is caused by low detection efficiency. Additionally, HPGe detectors require a cooling system during use, which increases the operational complexity and limits portability. This renders them unsuitable for rapid on-site measurements in specific scenarios [11]. In gamma scanning, the measurement accuracy, time efficiency, and detectable activity range are key performance indicators for detectors. Hence, $LaBr_3$(Ce) detectors, which have a 62% higher detection efficiency per unit volume than HPGe [12] detectors and a portable design, are more suitable.

Owing to the low energy resolution of $LaBr_3$(Ce) detectors and the inherent electronic noise in the spectrometer system, weak peaks in the complex spectrum are more susceptible to obscuring or overlapping. Therefore, to apply $LaBr_3$(Ce) detectors in the field of LILW and other low-activity radioactive material measurements, the crucial step in subsequent spectrum analysis is to adopt smoothing methods to effectively eliminate interfering signal components while preserving as much information as possible regarding the weak peaks in the low-count spectrum. Currently, the widely used traditional smoothing methods include the multi-point [13], Fourier transform, least squares [14, 15], polynomial fitting, and discrete function convolution sliding transform methods. However, traditional methods often distort valuable information contained in the original signal. Such distortion may result in problems such as the disappearance of weak peaks in the low-count spectrum, the emergence of false peaks, and compromised energy resolution. Additionally, certain

* This work was supported by the National Natural Science Foundation of China (No. 12405356), National Natural Science Foundation of China (No. 12075112), Hunan Provincial Natural Science Foundation Regional Collaborative Project (No. 2023JJ50121), and Hunan Provincial Department of Education Project (No. 23B0421)

† Corresponding author, yanghui@usc.edu.cn

traditional methods, including the Fourier transform, struggle to retain sudden variations in nonperiodic signals, such as the gamma spectrum. Compared with traditional methods, wavelet analysis, which has been increasingly applied to signal processing in recent years, employs discrete wavelet transform (DWT) for signal decomposition and reconstruction. This method enables the simultaneous analysis of signals in both the time and frequency domains, thereby accurately capturing detailed signal characteristics in multiple dimensions [16]. Additionally, because of the nonperiodic and finite energy characteristics of the mother wavelets used, this method exhibits substantial advantages in terms of information retention when applied to nonperiodic signal processing, such as speech signals [17, 18], radar signals [19], biomedical signals [20], and spectra [21]. Compared with other methods, it preserves information better [22]. Therefore, when smoothing the low-count gamma spectrum, wavelet analysis exhibits stronger performance advantages in extracting and preserving the parameters of weak peaks than traditional methods.

Smoothing methods based on wavelet analysis have been studied extensively. In terms of signal decomposition levels, Vilimek et al. [23] and Khalil et al. [24] empirically determined the optimal decomposition levels for different mother wavelets in DWT when addressing smoothing problems in image and biomedical signals, respectively. Yu et al. [25] processed a spectrum using different decomposition levels and achieved an optimal signal-to-noise ratio (SNR) of the reconstructed spectrum when the decomposition level was between 7 and 8. Cui and Li [26], He et al. [27], and Liu et al. [28] combined wavelet entropy and sample entropy (SE) theories to determine the optimal decomposition level when noise components are fully extracted by analyzing the chaos degree of detail coefficients at each level. However, in terms of maintaining weak peaks in the gamma spectrum, a research gap exists in the precise threshold criteria based on the signal reconstruction capability of smoothing methods. Regarding threshold calculation, researchers such as Poornachandra [29], Zhou [30], and Li et al. [31] established modified threshold models based on traditional threshold calculation formulas by studying the variation patterns of detail coefficients under wavelet transforms for single operating conditions, including white noise, colored noise, and the inherent noise of NaI(Tl) detectors. However, threshold correction under complex and multifaceted operating conditions has not been researched yet. In terms of threshold functions, Xiao et al. [32] smoothed the spectrum of Co-60 using both the five-point method and a nonlinear wavelet analysis technique. This preserved peak counts and the full width at half maximum (FWHM) of the full-energy peak effectively. However, the smoothness of this method is yet to be studied. Yan et al. [33] and Xie et al. [34] proposed a novel threshold function that combines the advantages of traditional soft and hard threshold functions. Meftah et al. [35] proposed a method based on the Donoho threshold model for smoothing the pressure signals from water pipe leaks. Mou et al. [36] constructed a novel three-segment threshold function based on seismic signal characteristics. Wei et al. [37], Liu et al. [38], and Pei et al. [39] replaced the threshold function with a neural network algorithm to modify wavelet coefficients. However, the threshold functions proposed in these studies are deficient in their capability of adaptive adjustment to a smooth low-count spectrum under complex operating conditions. Research on adjusting the wavelet coefficient shrinkage performance based on decomposition levels is insufficient.

In summary, several critical problems remain unresolved in the research on low-count gamma spectrum smoothing methods based on wavelet analysis. Consequently, when existing smoothing methods are applied to process a low-count gamma spectrum, substantial discrepancies occur between the smoothed spectrum and the original data, resulting in severe distortion of the characteristic peak shapes and a decrease in the peak-to-valley ratios. This further complicates the difficulty of resolving overlapping peaks. To address these problems, this study, for the first time, integrated the Nyquist sampling rate, Fourier transform, and SE to establish criteria for determining the optimal decomposition level and wavelet coefficient threshold under various complex operating conditions. A novel threshold function was constructed. Combined with the multi-point method, this threshold function becomes a technique for low-count gamma spectrum smoothing that ensures smoothness while strongly preserving the weak peaks and characteristic peak shapes in the spectrum. The results of this research provide a theoretical foundation and critical technical support for the application of $LaBr_3(Ce)$ detectors in the qualitative and quantitative analyses of LILW, thereby enhancing the safety of LILW disposal.

II. MATERIALS AND METHODS

Wavelet-based signal smoothing involves DWT decomposition to extract the wavelet coefficients, which are then shrunk to reduce the noise. The processed coefficients are then used to reconstruct the smoothed signals. Based on the discussion in Sec. I, the following problems occur when applying wavelet analysis to low-count spectrum analysis: First, the criterion for determining the optimal decomposition level based on the preservation of weak peaks has not been established. Second, current threshold models cannot adaptively adjust under complex working conditions. Third, precise threshold function models specifically designed for smoothing low-count gamma spectra are lacking. Hence, based on the key steps of DWT and the aforementioned problem, this section discusses the theoretical derivation, model establishment, and specific implementation process of the novel wavelet threshold multi-point method proposed in this paper. The section primarily discusses the derivation and establishment of three models: decomposition level, threshold correction, and threshold function models.

A. Decomposition level model

This paper integrates the Nyquist sampling rate [40] with SE theory [41]. It comprehensively considers the process of smoothing low-count gamma spectra, the impact of decom-

position levels on the preservation of weak peaks, and the effective elimination of noise. Thus, an improved criterion for determining the DWT decomposition level j is proposed, as shown in Eqs. (1) and (2),

$$j = \min\left\{j_{\mathrm{N}}, j_{\mathrm{S}}\right\}, \tag{1}$$

$$j_{\mathrm{N}} = \log_2 \frac{N^2}{2\sum_{k=0}^{N-1}\sum_{t=0}^{N-1} \mathrm{e}^{-i\frac{2\pi}{N}kt} y(t)} \tag{2}$$

where j denotes the optimal level of decomposition, and j_{N} and j_{S} represent the criteria for determining the optimal decomposition level of the low-count spectrum, derived from the integration of the Nyquist sampling rate and SE theory, respectively. j_{N} can be calculated using Eq. (2), whereas j_{S} must be obtained from the flowchart shown in Fig. 2, which is elaborated on in the subsequent sections.

The specific derivation process for j_{N} and j_{S} is as follows:

(1) Theoretical derivation and model establishment for j_{N}

When applying wavelet analysis for signal smoothing, we must first to perform decomposition using DWT with Eqs. (3) and (4):

$$\mathrm{DWT}[a,b] = \sum_{t=0}^{T-1} y(t)\cdot\psi_{a,b}[t] \tag{3}$$

$$\psi_{a,b}[t] = \frac{1}{\sqrt{a}}\psi\left(\frac{n-b}{a}\right) \tag{4}$$

where $\mathrm{DWT}[a,b]$ represents the coefficients of the discrete signal decomposed in the wavelet domain under scale parameter a and translation parameter b. $y(t)$ denotes a discrete signal. $\psi_{a,b}[t]$ denotes the mother wavelet.

First, we must conduct a layer-by-layer DWT decomposition process before reconstructing the original signal. At each decomposition layer, the signal must be calculated using Eq. (3), thus yielding the approximate coefficients C_j and detail coefficients D_j representing the effective and interference signal components, respectively. Simultaneously, at each decomposition layer, downsampling must be conducted with a sampling factor of 2 (i.e., sampling once for every two signal data points). Assuming that the original signal is a discrete signal $y(t)$ of length N, the process of layer-by-layer DWT decomposition is as illustrated in Fig. 1. Here, H_0 and H_1 represent high- and low-pass filters, respectively, as determined by the mother wavelet $\psi_{a,b}[t]$.

As shown in Fig. 1, with an increase in the decomposition level j, the sampling rate ω of a signal of length N decays exponentially by a factor of 2, as indicated by Eq. (5).

$$\omega = \frac{N}{2^j}, j = 1, 2, \ldots, n \tag{5}$$

Moreover, according to the Nyquist sampling rate requirement, if the original signal is to be recovered, the sampling frequency of the signal must not be less than twice

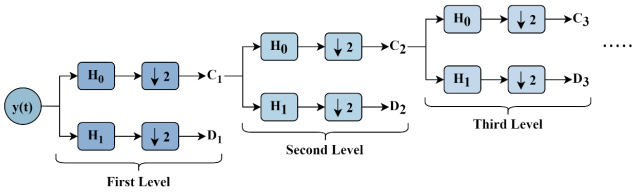

Fig. 1. (Color online) Schematic of DWT processing on the original signal $y(t)$

the maximum frequency component of the signal. This implies that the number of layers required to perform the DWT on the original signal cannot exceed the maximum number of layers determined by the Nyquist sampling rate requirement. Because high-frequency components in the gamma spectrum often constitute noise that must be eliminated during the smoothing process, the proposed smoothing method need not consider the ability to retain the reconstruction of the maximum frequency component. Therefore, the average frequency of the gamma spectrum is used as the primary retention target, thereby replacing the maximum frequency. If the average frequency component of the gamma spectrum is denoted by $\bar{\omega}$ (obtained by taking the mean value through the discrete Fourier transform of the gamma spectrum [42]), and the minimum sampling rate for the energy spectrum is denoted by ω_{s}. According to the Nyquist sampling rate theorem,

$$\omega \geq \omega_{\mathrm{s}} \tag{6}$$

$$\omega_{\mathrm{s}} = 2\bar{\omega} \tag{7}$$

$$\bar{\omega} = \frac{1}{N}\sum_{k=0}^{N-1}\sum_{t=0}^{N-1} \mathrm{e}^{-i\frac{2\pi}{N}kt} y(t) \tag{8}$$

Hence, based on Eqs. (6)–(8), the maximum decomposition level, denoted as j_{N}, determined using the Nyquist sampling rate, can be calculated using the following formula:

$$j_{\mathrm{N}} = \log_2 \frac{N^2}{2\sum_{k=0}^{N-1}\sum_{t=0}^{N-1} e^{-i\frac{2\pi}{N}kt} y(t)} \tag{9}$$

(2) Theoretical derivation and model establishment for j_{S}

SE is a measure used to characterize the complexity and disorder of time-series signals. A higher SE of each layer's detail coefficients D_j, which contain noise components from the gamma spectrum, indicates greater noise content in the detail coefficients of that layer. Additionally, as the number of decomposition layers increases, the noise components extracted via DWT gradually decrease. At a certain level of decomposition, the noise components no longer undergo changes. Therefore, by calculating the SE of each D_j, we can determine whether the noise components in the signal have been completely extracted.

The SE is calculated as follows: We consider a discrete-time sequence of length N, denoted by $y(t) = \{y_1, y_2, y_3, \cdots, y_N\}$. Additionally, we define a set of m-dimensional vector groups $\{y_m(1), y_m(2), y_m(3), \cdots, y_m(N-m+1)\}$, where $y_m(i) = \{y(1), y(2), y(3), \cdots, y(i+m-1)\}$. The formulas for calculating SE are given in Eqs. (10)–(12).

$$\mathrm{SE}(m, r, N) = -\ln\left[\frac{B^{m+1}(r)}{B^m(r)}\right] \tag{10}$$

$$B^m(r) = \frac{1}{N-m}\sum_{i=1}^{N-m} B_i^m(r) \tag{11}$$

$$B^{m+1}(r) = \frac{1}{N-m}\sum_{i=1}^{N-m} B_i^{m+1}(r) \tag{12}$$

Here, B_i represents the number of vectors $y_m(j)$ whose maximum distance from $y_m(i)$ is less than the tolerance value (where $1 \le j \le N-m+1$ and $j \ne i$). Typically, m and r are set to $m = 2$ and $r = 0.2\sigma$, respectively. Based on the SE theoretical principles and calculation process, Fig. 2 shows a flowchart for determining the adequacy of the noise-component extraction by calculating the SE values of the wavelet coefficients obtained from the gamma spectrum at various DWT levels.

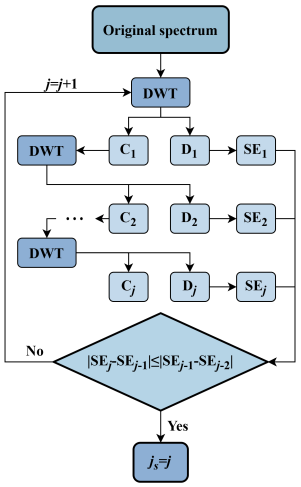

Fig. 2. (Color online) Flowchart for calculating j_S

As shown in Fig. 2, the SE is calculated for the detail coefficients of each layer obtained after decomposing the original spectrum via DWT. Thereafter, the variation pattern of the absolute difference in the SE between adjacent layers is analyzed. The optimal decomposition level, denoted by j_S, is reached when the absolute difference reaches its minimum value.

B. Threshold correction model

After DWT is implemented on the signal, wavelet coefficients encompassing valid signals must be discriminated from those representing interference, within a specified threshold. Based on the DWT theoretical principles outlined in Sec. II A, after decomposition at various levels, the characteristic peaks of radionuclides in the gamma spectrum are concentrated in the wavelet coefficients above the threshold, whereas the noise components are predominantly found in the coefficients below this threshold. According to the traditional estimation formula for a fixed threshold t given by Dohono,

$$t = \sigma\sqrt{2\ln(N)} \tag{13}$$

$$\sigma = \sqrt{\frac{1}{n}\sum D_1^2} \tag{14}$$

where N represents the length of the signal, and σ denotes the noise energy obtained by calculating the standard deviation of the detail coefficients from the first level of decomposition. However, the detail coefficients D_j, which represent noise components, vary with the decomposition level. Using this fixed threshold to discriminate wavelet coefficients often leads to substantial errors, resulting in problems such as misidentification of effective signals as interference signals. Hence, this study developed a threshold correction model by considering the variation pattern of the coefficients corresponding to different frequency signal components in the wavelet domain of the low-count gamma spectrum relative to the decomposition level:

$$t_1 = t \tag{15}$$

$$t_{j+1} = \mu t_j, j = 1, 2, \ldots, n \tag{16}$$

The threshold correction formula is recursive, where the initial value t_1 represents the threshold for the first-level coefficients, which is calculated using the traditional threshold formula. This initial value is then adjusted using the coefficient μ to obtain the thresholds t_j for subsequent wavelet coefficient levels. The detailed derivation and calculation processes are as follows.

Based on the theoretical principles of DWT, when applied to gamma spectrum analysis, it decomposes the original signal into a wavelet basis formed by translating the mother wavelet into the energy domain. In addition, as described in Sec. II A, during the implementation of DWT on the original gamma spectrum, each level of decomposition is accompanied by a downsampling step with a sampling factor of 2. Consequently, as the decomposition level increases, the frequency of the wavelet basis onto which the original signal is decomposed decreases exponentially by a factor of 2. Thus, the relationship between the frequency of the wavelet basis at each decomposition level and level j can be described using Eq. (17):

$$\omega_j = \frac{N}{N_{\text{wavelet}} \cdot 2^{j-1}} \tag{17}$$

where N is the length of the signal, ω_j is the frequency of the signal extracted from the jth layer, and N_{wavelet} is the length of the mother wavelet. Combined with the spectrum $y(\omega)$ obtained by performing the FFT on the original gamma spectrum $y(t)$, the relationship between the amplitude values of the frequency components extracted from adjacent decomposition levels j is described as follows:

$$\mu = \frac{y\left(\omega_{j+1}\right)}{y\left(\omega_j\right)} \tag{18}$$

Based on the theoretical principles of DWT, the amplitude values of various frequency components $y\left(\omega_j\right)$ should be directly proportional to their corresponding wavelet coefficients in the wavelet domain. Consequently, by substituting the coefficient μ, calculated using Eqs. (17)-–(18) into recursive Eqs. (15)–(16), the wavelet coefficient thresholds for adjacent levels can be adjusted. Using the aforementioned modified threshold model based on the coefficient μ, the wavelet coefficient thresholds at each decomposition level can be adaptively adjusted based on the actual variation patterns of the wavelet coefficients during the layer-by-layer DWT decomposition. This effectively addresses the problem of misjudgment of valid signals that may result from traditional fixed-threshold methods.

To verify the accuracy of the correction coefficient, we developed a μ model. DWT was performed on a gamma spectrum labeled Co-60-n with different counts. The specific experimental conditions for Co-60-n are described in Sec. III and Table 1. The theoretical proportional values of the wavelet coefficients at each level were calculated using the μ model. Fig. 3 compares the calculated and actual values of the proportion of the wavelet coefficients across each level.

As shown in Fig. 3, the calculated μ values exhibited a variation trend consistent with the actual wavelet coefficients across different decomposition levels. Thus, through the implementation of the threshold correction model μ presented in this paper, the adjustment of thresholds for each level is practicable, which corresponds with the variations in wavelet coefficients across different count scenarios.

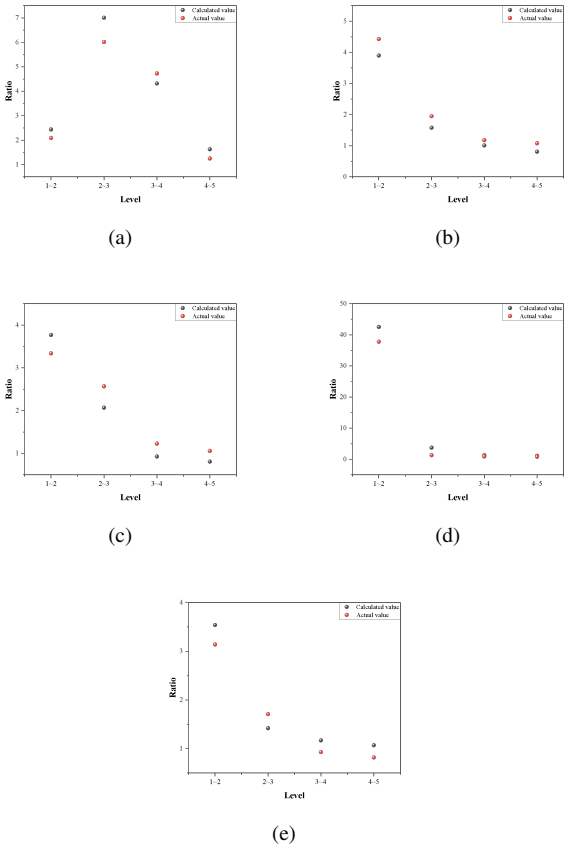

Fig. 3. (Color online) (a) to (e) Comparison of the actual and calculated μ values for Co-60-1 to Co-60-5 gamma spectra, respectively

C. Novel threshold function model

A crucial aspect of DWT for signal smoothing is the processing of wavelet coefficients representing both valid and interference signals through a threshold function. This aims to preserve the wavelet coefficients of valid signals as accurately as possible while suppressing those of interference signals. Traditional soft and hard threshold functions are represented by Eqs. (19) and (20), respectively:

$$\hat{W}_{j,k} = \begin{cases} \operatorname{sgn}\left(W_{j,k}\right)\left(\left|W_{j,k}\right| - t\right), \left|W_{j,k}\right| \geqslant t \\ 0, \left|W_{j,k}\right| < t \end{cases} \tag{19}$$

$$\hat{W}_{j,k} = \begin{cases} W_{j,k}, \left|W_{j,k}\right| \geqslant t \\ 0, \left|W_{j,k}\right| < t \end{cases} \tag{20}$$

where $W_{j,k}$ represents the original wavelet coefficients, and $\hat{W}_{j,k}$ denotes the wavelet coefficients after shrinkage processing. The variable t refers to the fixed threshold mentioned in Sec. II B. However, during the processing of wavelet coefficients using traditional soft and hard threshold functions, problems such as data oscillations and fixed errors often occur during the signal reconstruction phase [43]. This renders the spectrum highly susceptible to the loss of weak peaks when applied to low-count spectrum smoothing. To address the limitations of traditional soft and hard threshold functions, we propose a novel threshold function, shown in Eq. (21): Graphs representing traditional soft and hard threshold functions, as well as the novel threshold function, are shown in Fig. 4.

As shown in Fig. 4, the traditional soft, hard, and novel threshold functions all process wavelet coefficients smaller than the threshold by shrinkage and strive to maintain wavelet coefficients larger than the threshold close to their original values, thus eliminating noise while preserving valid signals. However, the primary advantages of the novel threshold function over traditional ones are as follows:

(1) Unlike traditional soft and hard threshold functions, which have discontinuities at the threshold t, the novel threshold function and its first derivative both demonstrate excellent

$$\hat{W}_{j,k}\begin{cases}\left(|W_{j,k}|-\frac{1}{|W_{j,k}|^{j}}+t_j\left(\frac{t_j}{t_j+\frac{1}{j}}\right)^{n}-t_j+\frac{1}{t_j{}^{j}}\right)\operatorname{sgn}(W_{j,k}),|W_{j,k}|\geqslant t_j\\ t_j\left(\frac{|W_{j,k}|}{t_j+\frac{1}{j}}\right)^{n}\operatorname{sgn}(W_{j,k}),|W_{j,k}|<t_j\end{cases}\tag{21}$$

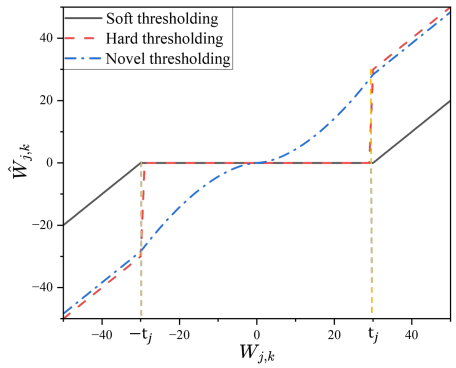

Fig. 4. (Color online) Comparison of traditional soft, hard, and novel threshold functions

continuity at t. This characteristic ensures that the signal reconstructed after processing with the novel threshold function does not exhibit oscillatory behavior.

(2) For wavelet coefficients below the threshold, the traditional soft and hard threshold functions directly set them to zero, whereas the novel threshold function employs a flexible shrinkage strategy that gradually reduces the coefficients from strong to weak. This characteristic enables the novel threshold function to achieve a shrinkage effect on the wavelet coefficients that aligns with their variation patterns under a layer-by-layer decomposition in DWT.

(3) When the wavelet coefficients exceed the threshold, as the original wavelet coefficient $W_{j,k}$ increases, the error between the processed threshold $\hat{W}_{j,k}$ from the novel threshold function and the original wavelet coefficient $W_{j,k}$ gradually decreases, enabling better preservation of the low-frequency components corresponding to the characteristic peaks of nuclides in the gamma spectrum.

Eq. (21) shows that the novel threshold function utilizes the parameters j and N to adjust the degree of wavelet coefficient shrinkage at different decomposition levels j. Here, t_j represents the wavelet threshold for each level, which is accurately calculated using the threshold correction formula described in Sec. II B. Additionally, as the decomposition level j increases, the degree of shrinkage gradually decreases. This characteristic enables the novel threshold function to better adapt to the varying noise components in DWT, which decrease with increasing decomposition levels. Consequently, compared with traditional threshold functions, the novel threshold function demonstrates superior performance in eliminating noise while preserving weak signals.

The aforementioned characteristics of the novel threshold function effectively address the problems of data oscillation and fixed errors encountered in the signal reconstruction stage using traditional soft and hard threshold functions, which occur because of their noncontinuity and rigid shrinkage properties.

D. Smoothing process of the novel wavelet threshold multi-point method

Based on the preliminary theoretical and experimental research conducted in this study, wavelet analysis, despite its notable advantages in preserving signal characteristic parameters, exhibited limitations in terms of smoothness. To compensate for this inherent limitation of wavelet analysis, we innovatively integrate the multipoint smoothing method, known for its superior smoothing properties, with the models established in Sec. II A–II C. Thus, we propose a novel wavelet threshold multi-point method for a low-count gamma spectrum, which combines the capability of wavelet analysis to preserve weak signals with the excellent smoothing effects of the multi-point method.

The multi-point method is a traditional smoothing technique that is widely utilized in gamma-spectrum signal processing (as exemplified by its adoption in the renowned spectrum analysis software Gamma Vision [44]). It induces substantial distortion in the peak shapes of the original gamma spectrum during the smoothing process, potentially leading to the loss of weak peaks. However, research indicates that the multi-point method exhibits remarkable superiority in enhancing the smoothness of the spectrum compared with alternative approaches. Assuming y_i represents the count of the i-th channel in the gamma spectrum, the centroid position between the i-th and $(i+1)$-th channel counts can be computed using the following formula [45]:

$$\bar{y}_{i+0.5}=\frac{1}{2}\left(y_i+y_{i+1}\right)\tag{22}$$

$$\bar{y}_{i-0.5}=\frac{1}{2}\left(y_{i-1}+y_i\right)\tag{23}$$

Consequently, we can deduce that

$$\bar{y}_i=\frac{1}{2}\left(\bar{y}_{i+0.5}+\bar{y}_{i-0.5}\right)=\frac{1}{4}\left(y_{i-1}+2y_i+y_{i+1}\right)\tag{24}$$

$$\bar{y}_i=\frac{1}{16}-\left(y_{i-2}+4y_{i-1}+6y_i+4y_{i+1}+y_{i+2}\right)\tag{25}$$

Equations (24) and (25) represent the three- and five-point multi-point methods, respectively.

The gamma-spectrum smoothing process utilizing the novel threshold function integrated with the multi-point

method is illustrated in Fig. 5. Initially, the original gamma spectrum $y(t)$ undergoes FFT and DWT for layer-by-layer decomposition, yielding its frequency spectrum and wavelet coefficients $W_{j,k}$ (including the approximation and detail coefficients C_j and D_j). Subsequently, using the optimal decomposition level criterion proposed in Sec. II A, we can calculate the SE SE_j of each layer's detail coefficient D_j. When the difference in SE between the j-th and $(j-1)$-th layers' detail coefficients is less than the difference in SE between any of the preceding adjacent layers up to the $(j-1)$-th layer, or when the layer number j exceeds the maximum decomposition level j_{N} determined by the Nyquist sampling rate theorem in Sec. II A, the decomposition process is terminated. Next, the threshold correction model presented in Sec. II B is used to compute the wavelet coefficient thresholds for each layer. These thresholds are then incorporated into the novel threshold function proposed in Sec. II C. The modified coefficients $\hat{W}_{j,k}$ are obtained by performing a shrinkage process on the wavelet coefficients $W_{j,k}$ of each layer. Finally, the modified wavelet coefficients $\hat{W}_{j,k}$ are utilized to reconstruct the gamma spectrum layer-by-layer, resulting in the reconstructed energy spectrum $y'(t)$. Subsequently, the multi-point method is applied to further process $y'(t)$, yielding the final smoothed gamma spectrum $y''(t)$.

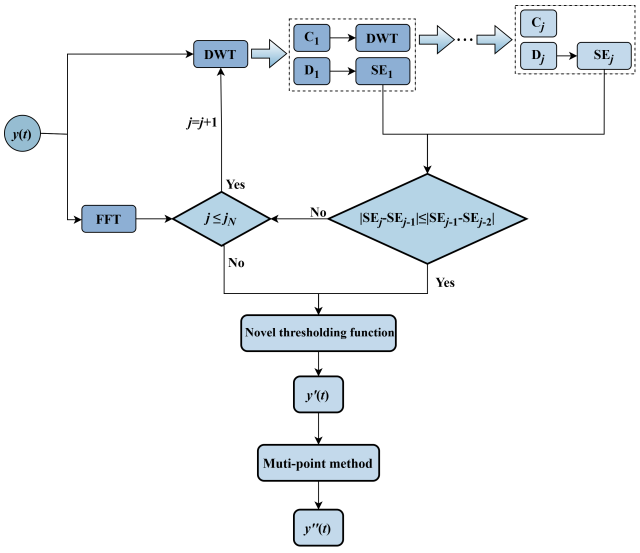

Fig. 5. (Color online) Spectrum smoothing process of the novel threshold multi-point method

The innovation of the proposed method, as illustrated in the technical roadmap of Fig. 5, lies primarily in the utilization of the modified threshold model and threshold function proposed in Sec. II B and II C, respectively, during the key steps for determining the optimal DWT decomposition level and performing wavelet coefficient shrinkage and reconstruction. As described in Sec. II B and II C, the specific advantages of the novel threshold model include its ability to adjust the thresholds at different decomposition levels and the adoption of the flexible shrinkage of wavelet coefficients based on specific operating conditions. These advantages effectively prevent the loss of weak peaks in the gamma spectrum during the smoothing process, which can occur because of the misidentification and elimination of the characteristic peaks of radionuclides as noise.

E. Experimental conditions

The $\mathrm{LaBr_3}$(Ce) detector used in the experiments was manufactured by ORTEC, and featured a crystal produced by Saint-Gobain. The integrated multi-channel analyzer, along with the detector and its assembly, is shown in Fig. 6. The $\mathrm{LaBr_3}$(Ce) detector was housed within a lead shield during the gamma spectrum measurements to mitigate the impact of environmental and cosmic radiation on the measurement outcomes. Before the measurements, rigorous internal radioactivity elimination and sample normalization procedures were conducted according to the specifications outlined in the IEC 61453:2007 standard [46]. The radionuclide selected for this study was Co-60, a crucial fission and activation product [47, 48]. The Co-60 radioactive source used in the experiments is shown in Fig. 6. The calibration measurement duration was set to exceed 60 s, and the measurements were conducted at a constant temperature of 25.0 degreeCelsius to eliminate the need for temperature correction.

Fig. 6. (Color online) Low-background environmental gamma spectrometer system and Co-60

Owing to the difficulties in acquiring a measured gamma spectrum with overlapping peaks of varying peak distances under low-count conditions, this study employed a method of simulating a low-count spectrum through the superposition of Gaussian functions with white noise [49]. The measured and simulated low-count Co-60 gamma spectrum are shown in Fig. 7. The model used to simulate the gamma spectrum was implemented in MATLAB R2023a.

As depicted in Fig. 7, the simulated gamma spectrum generated using this method exhibited consistent characteristic peak shapes (peak counts, full-width at tenth-maximum (FWTM)) with the measured spectrum. The primary discrepancy resulted from the noise distribution in the measured spectrum not perfectly conforming to the characteristics of white noise with a normal distribution. The proposed method considers diverse noise distributions in the gamma spectrum under various operating conditions. Consequently,

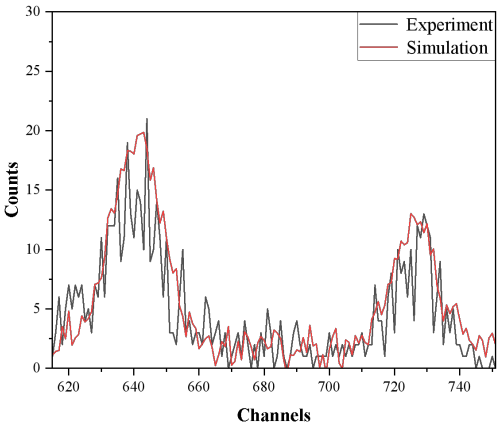

Fig. 7. (Color online) Comparison of simulated and measured gamma spectrum

the low-count gamma spectrum obtained using this simulation method was consistent with the measured spectrum, validating the smoothing performance of the novel method.

III. RESULTS AND DISCUSSION

We aimed to validate the smoothing performance of the novel threshold multi-point method under low-energy-resolution conditions for a low-count gamma spectrum. A $LaBr_3$(Ce) detector was employed to measure the standard point source of a critical nuclide Co-60. By adjusting the distance between the point source and detector probe (at 25 , 50 , 75 , 100 , and 125 cm), we obtained one high-count gamma spectrum (numbered as 1) and four low-count gamma spectrum (numbered as 2 to 5). Five smoothing methods were applied to process the spectrum of varying counts: the traditional five-point, soft thresholding, hard thresholding, novel threshold, and novel threshold multi-point methods. The comparative performance indicators evaluated for these methods in smoothing both high- and low-count gamma spectra were the smoothness, root mean square error (RMSE), SNR [50], and FWTM.

A. Optimal value of the correction factor N in the novel threshold function

As outlined in Sec. II C, the threshold correction factor N in the novel threshold function influences the extent of shrinkage applied to the wavelet coefficients. Moreover, the optimal value of N varies for different total counts and energy spectrum smoothing objectives. Before conducting comparative experiments on the smoothing effects of different methods on the gamma spectrum, we initially conducted a preliminary investigation into the optimal value of N in the novel threshold function. By analyzing the variation patterns of the smoothness of the gamma spectrum and the RMSE between the original and smoothed gamma spectra, we determined the optimal value of N. The results are presented in Fig. 8. The meaning of the notation "Co-60-n" in the Fig. 8 is described in Table 1, which lists the detection distance, temperature, time, and total count corresponding to the spectra denoted by various notations.

TABLE 1. Information of measured gamma spectrum Co-60-n

Notation	Nuclide	Detector distance (cm)	Detector temperature (°C)	Detector time (s)	Total counts
Co-60-1		25			240517
Co-60-2		50			2201
Co-60-3	Co-60	75	25	120	886
Co-60-4		100			656
Co-60-5		125			386

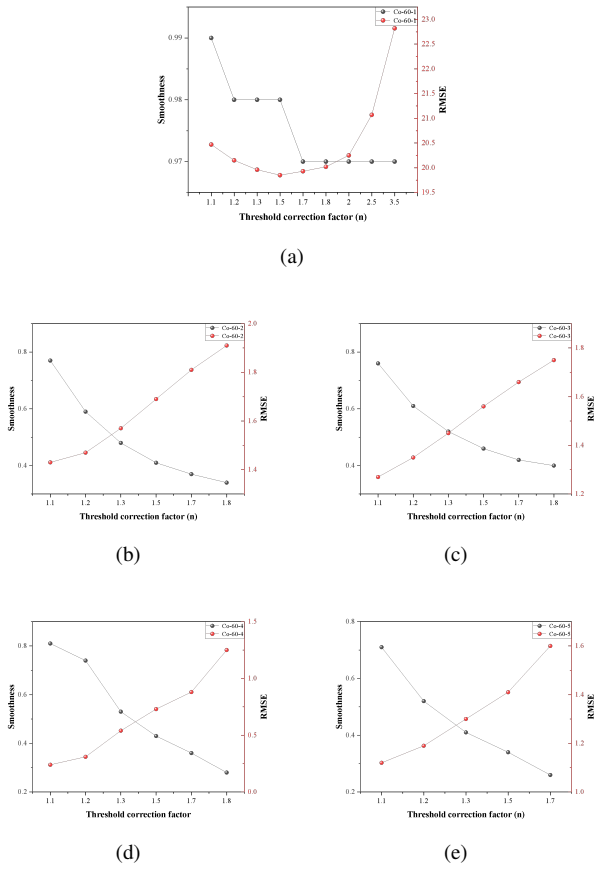

Fig. 8. (Color online) (a) to (e) Variation trends of smoothness and RMSE with the parameter N for the spectrum with high and low counts

As depicted in Fig. 8, with the variation in N, the smoothness and RMSE exhibited decreasing and increasing trends, respectively. Specifically, a decrease in smoothness indicates an enhancement in the degree of smoothing of the gamma spectrum. Conversely, the increase in RMSE values suggests an amplification of the difference between the original and

smoothed gamma spectra. To balance the smoothness and weak signal preservation capabilities of the novel threshold function, we determined the optimal value of N as the intersection point of the smoothness and RMSE curves.

Consequently, as illustrated in Fig. 8(a), the optimal range for N of the novel threshold function for the high-count gamma spectrum was between 1.8 and 2.0. Furthermore, as shown in Figs. 8(b)–8(e), the optimal range for N of the novel threshold function for the low-count gamma spectrum was between 1.2 and 1.4. Consequently, when smoothing low-count gamma spectrum, to ensure both the smoothing capability and weak signal preservation of the novel threshold function, we set N to the median value of 1.3 within its optimal range of 1.2 to 1.4. At this value, the relative errors of the optimal values of smoothness and RMSE for various count gamma spectra processed by the novel threshold function were 0.08 and 0.03, respectively. This indicated that adopting a median value of 1.3 for the optimal N provides a certain degree of precision.

B. Preservation capability of weak peaks of critical nuclides in novel methods

Smoothing treatments were applied to various groups of the gamma spectrum using five distinct approaches: the traditional multi-point, soft thresholding, hard thresholding, novel threshold, and novel threshold multi-point methods. Table 2 presents the SNR values of the smoothed spectrum, RMSE values between the original and smoothed spectra, and smoothness and FWTM values of the characteristic peaks in the smoothed spectrum, all of which were obtained after applying the aforementioned denoising methods to spectra with different counts.

Analysis of the data presented in Table 2 shows that all five methods effectively enhanced the SNR of the original gamma spectrum. In particular, the novel thresholding method emerged as the most effective, followed by the novel threshold multi-point method, achieving SNR improvements of 3.10 and 2.51 times, respectively. Compared with traditional methods, the novel thresholding function exhibited superior performance in terms of noise reduction. In terms of smoothness and RMSE values, the soft thresholding method yielded the lowest smoothness value of 0.01 for the low-count gamma spectrum, followed by the novel threshold multi-point method at 0.07. A lower smoothness indicates better smoothing performance of the method. However, excessively low smoothness may lead to the loss of a weak peak in the gamma spectrum. Consequently, to evaluate the smoothing performance of the methods comprehensively, we must consider both the smoothness and RMSE values. Referring to the denoising results labeled 5 in Table 2, when denoising the low-count spectrum with a total peak count of 386, the RMSE values for the soft threshold and novel methods were 10.87 and 1.40, respectively. Compared with the traditional threshold method, the novel threshold multi-point method achieved a reduction of 87.1%. This suggests that the novel threshold multi-point method, while maintaining high smoothing capabilities, minimizes the differences between the smoothed and original gamma spectra compared with other methods. Regarding the FWTM variations in the characteristic peaks before and after smoothing, traditional methods typically resulted in changes of eight to 33 channels, whereas the novel threshold multi-point method exhibited minimal FWTM variations within the range of one to two channels. Consequently, the novel threshold multi-point method not only effectively removes noise components but also, when applied to low-count gamma spectrum smoothing, achieves minimized RMSE values while maintaining superior weak peaks and characteristic peak shape preservation performance compared to other methods. Furthermore, its smoothness was further improved compared with using the novel thresholding method without incorporating the multi-point method.

To clearly demonstrate the comprehensive advantages of the novel threshold multi-point method when applied to smoothing low-count gamma spectra, we performed a comparative analysis of the high- and low-count gamma spectra before and after smoothing using the traditional hard and soft thresholding and novel threshold multi-point methods. The results are shown in Fig. 9.

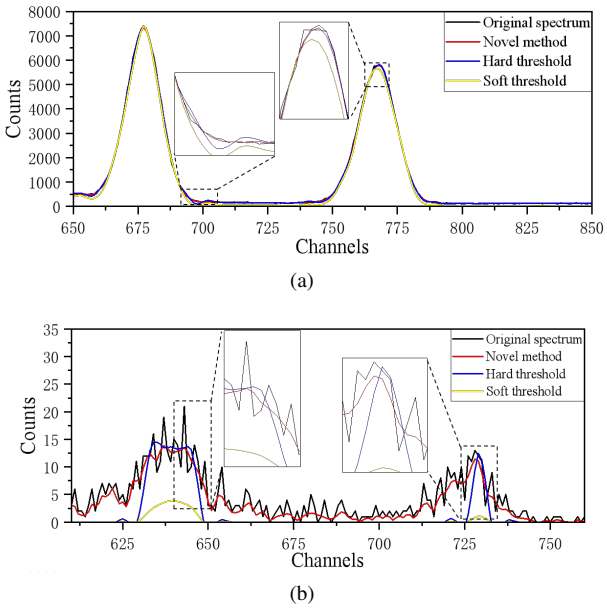

Fig. 9. (Color online) Comparison of (a) high-count and (b) low-count Co-60 gamma spectrum after processing with traditional hard, soft, and novel threshold functions

As shown in Fig. 9(a), compared with the hard thresholding and novel threshold multi-point method, the soft thresholding method introduced a certain fixed error between the peak counts of the smoothed and original spectra. Through a comparative analysis of the characteristic peak boundaries before and after smoothing, we observed that the spectrum processed by the novel threshold multi-point method exhibited the highest similarity in peak shape at the characteristic peak boundaries with the original spectrum, indicating its superior peak shape preservation capability. Figure 9(b) reveals

TABLE 2. Parameters of original and smoothed spectra using different methods

Number	Counts	Method	SNR (dB)	RMSE	Smoothness	FWTM (Channel)
1	240517	Original spectrum	20.86			60
		Multi-point	31.24	34.54	0.77	47
		Hard threshold	28.82	37.48	0.94	41
		Soft threshold	23.35	70.30	0.94	42
		Novel threshold	33.82	21.07	0.97	60
		Novel threshold multi-point	35.45	17.46	0.92	58
2	2201	Original spectrum	−7.92			54
		Multi-point	10.14	14.42	0.22	52
		Hard threshold	10.35	3.24	0.26	56
		Soft threshold	5.81	5.47	0.12	56
		Novel threshold	16.66	1.57	0.48	55
		Novel threshold multi-point	11.97	2.69	0.21	54
3	886	Original spectrum	−13			38
		Multi-point	10.01	12.88	0.25	46
		Hard threshold	6.07	2.86	0.23	35
		Soft threshold	2.48	4.33	0.13	35
		Novel threshold	12.59	1.35	0.61	39
		Novel threshold multi-point	9.58	1.91	0.13	39
4	656	Original spectrum	−16			44
		Multi-point	9.59	13.51	0.24	53
		Hard threshold	8.03	1.87	0.43	31
		Soft threshold	3.19	3.26	0.17	19
		Novel threshold	16.15	0.73	0.43	44
		Novel threshold multi-point	14.96	0.84	0.16	45
5	386	Original spectrum	−17			54
		Multi-point	9.96	12.89	0.26	56
		Hard threshold	12.12	10.06	0.12	22
		Soft threshold	11.44	10.87	0.01	21
		Novel threshold	13.18	8.90	0.55	54
		Novel threshold multi-point	9.11	1.40	0.07	54

that the traditional hard and soft thresholding methods introduced substantial distortions in both the peak counts and peak boundaries of the Co-60 characteristic peaks when applied to low-count gamma spectrum smoothing. In contrast, the novel threshold multi-point method, when applied to a low-count gamma spectrum, effectively maintained the smoothness of the smoothed spectrum while preserving the characteristic peak shapes with a higher degree of fidelity. This may be owing to the adaptive adjustment capability of the threshold calculation and threshold function model employed in the novel method. This model performs adjustments based on specific operating conditions and total count level in the peak spectral region. Thus, it averts the common pitfall of traditional threshold methods, where effective signals are erroneously discarded as noise owing to inappropriate wavelet coefficient shrinkage. Hence, Fig. 9 reveals that compared with the traditional threshold, the novel method is better in preserving radionuclide characteristic peak shapes, such as peak counts and widths, when applied to gamma spectrum smoothing.

In summary, when applied to the smoothing of low-count gamma spectra, compared with the other four traditional methods, the threshold multi-point method achieves minimal differences between smoothed and original spectra while effectively removing noise. Moreover, it demonstrates a more pronounced capability in preserving the characteristic peak shapes. Additionally, the integration of the novel threshold function with the multi-point method further enhances the smoothness of the novel threshold function compared with the traditional threshold function.

C. Influence of the novel method on the peak-to-valley ratio of overlapping peaks

The complex spectra of LILW often contain numerous overlapping peaks that tend to undergo a reduction in the peak-to-valley ratio (ratio of peak counts to valley counts in overlapping peaks) during smoothing, as indicated by the blue dashed line in Fig. 10(a). This reduction can exacerbate the challenge of accurately resolving overlapping peaks in subsequent spectrum-unfolding processes [51].

To investigate the impact of the novel method on the peak-to-valley ratio of overlapping peaks in a complex low-count gamma spectrum, this study employed both traditional methods and the novel threshold multi-point method to smooth overlapping peaks with varying peak distances. A comparative analysis was then conducted to assess the changes in the peak-to-valley ratio before and after smoothing using each method. Using the simulated gamma spectrum method outlined in Sec. II E, we simulated a low-count overlapping peak spectrum with a peak area ratio of $1:1$ and varying peak dis-

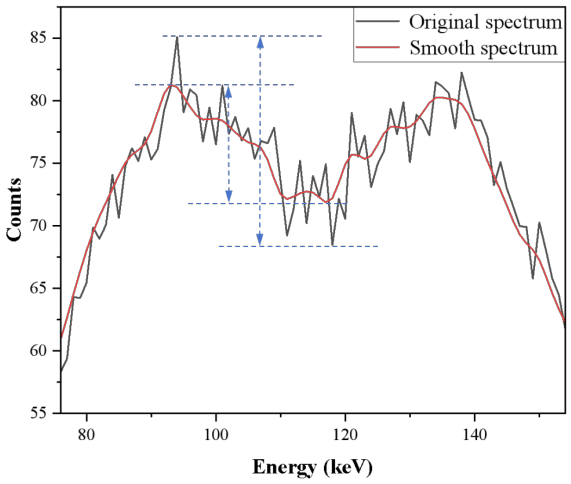

(a)

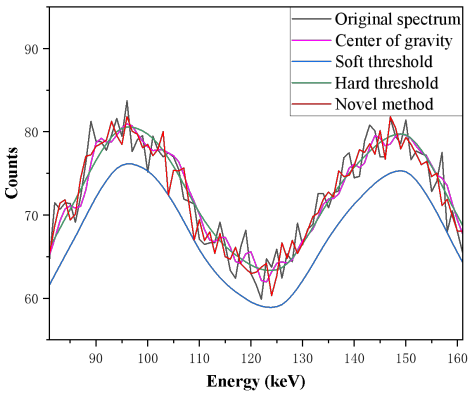

(b)

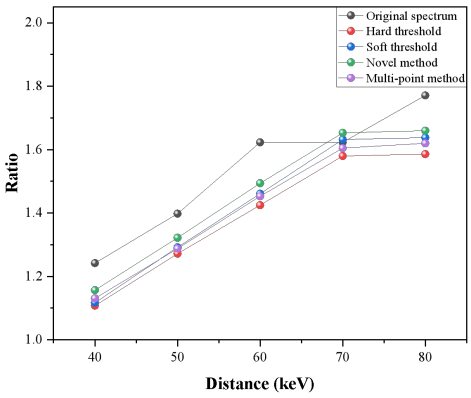

(c)

Fig. 10. (Color online) (a) Comparison of overlapping peaks in gamma spectrum before and after smoothing; (b) comparison of overlapping peak in low-count spectrum smoothed by various methods; (c) peak-to-valley ratios of overlapping peaks in low-count spectrum after applying various smoothing methods across different peak distances

tance. These spectra were then subjected to smoothing using the traditional five-point, hard thresholding, soft thresholding, and novel threshold multi-point methods. The resulting spectra are shown in Figs. 10(b)—Fig. 10(c).

As shown in Fig. 10(b), the novel method minimized the discrepancies in the peak and trough counts of the overlapping peaks between the original and smoothed spectra compared with other methods. Based on the results presented in Fig. 10(c), for all peak distances, the peak-to-valley ratios of the overlapping peaks smoothed using the novel method were higher than those of the other methods, with a maximum improvement of 7.4%. Note that although the peak-to-valley ratios of the overlapping peaks in the smoothed gamma spectrum generally decreased compared with the original spectrum, the influence of the novel threshold multi-point method on the peak-to-valley ratio was substantially smaller than that of the other methods. Notably, when the peak distance was 70 keV, smoothing the spectrum with the novel threshold multi-point method resulted in an increase in the peak-to-valley ratio of overlapping peaks by 0.05 compared with the original spectrum. Therefore, based on the results shown in Figs. 10(b) and 10(c), we can conclude that the novel method effectively mitigates the reduction in the peak-to-valley ratio observed in the smoothed overlapping peaks of the low-count spectrum compared with the other methods.

IV. SUMMARY

Traditional methods for smoothing low-count gamma spectra have some limitations, such as poor information preservation, substantial distortion of weak peaks, and reduced peak-to-valley ratios in overlapping peaks. Hence, this study innovatively integrated the Nyquist sampling theorem, FFT, and DWT and examines the characteristics of weak peaks and noise components in the low-count gamma spectrum, both in the energy and frequency domains. It revealed the intricate interplay between detail coefficients, approximation coefficients, and thresholding in DWT for low-count gamma spectra. Based on this, criteria for determining the number of DWT decomposition levels, as well as a threshold correction model and threshold function, were established. Moreover, a novel threshold multi-point method for smoothing low-count gamma spectra was developed. This method has substantial advantages in terms of smoothness, SNR, RMSE, and the preservation of characteristic peak shapes. Through both theoretical and experimental investigations, the following conclusions were drawn:

(1) For information preservation and noise elimination, both traditional and novel methods were employed to smooth the high- and low-count spectra of critical nuclides. The results indicated that the application of the novel threshold multi-point method substantially enhanced the SNR by 2.51 times. Furthermore, it achieved a lower smoothness of 0.07 while reducing the RMSE by 87.1% compared with traditional approaches.

(2) In terms of the retention of the characteristic peak shapes, both traditional and novel methods were utilized for noise reduction in the high- and low-count spectra of key nuclides. The results revealed that traditional smoothing methods caused shifts in the FWTM values of the characteristic peaks, ranging from 8 to 33 channels, compared with the original spectrum. Conversely, the novel threshold multi-point method exhibited minimal FWTM distortions of only 1–2 channels, representing a reduction of 75.0% to 96.9% compared with traditional methods.

(3) In terms of the impact on the peak-to-valley ratio of overlapping peaks, the multi-point, traditional thresholding, and novel threshold multi-point methods were applied to a smooth low-count overlapping gamma spectrum with a peak area ratio of $1:1$ and varying peak distances. Across all peak distances, the spectrum processed using the novel threshold multi-point method consistently exhibited superior peak-to-valley ratios compared with other methods. Notably, the peak-to-valley ratio was improved by up to 0.074 compared with alternative approaches. Specifically, at a peak distance of 70 keV, the peak-to-valley ratio of the overlapping peaks enhanced by the novel threshold multi-point method surpassed that of the original spectrum by 0.05.

[1] International Atomic Energy Agency, Interim storage of radioactive waste packages (IAEA publishing, 1998). https://www.iaea.org/publications/5724/interim-storage-of-radioactive-waste-packages

[2] V.M. Efremenkov, Radioactive waste management at nuclear power plants (IAEA publishing Bulletin, 1989). https://www.iaea.org/sites/default/files/publications/magazines/bulletin/bull31-4/31404683742.pdf

[3] International Atomic Energy Agency, Radioactive waste management status and trends (IAEA publishing, 2001). https://www-pub.iaea.org/MTCD/publications/PDF/wmdb-st-1/IAEA-WMDB-ST-1-1.PDF

[4] M.S. Yim, *Nuclear Waste Management* (Springer, Dordrecht, 2022), p. 635. doi:10.1007/978-94-024-2106-4

[5] International Atomic Energy Agency, Predisposal management of radioactive waste (IAEA Publishing, 2009). https://www-pub.iaea.org/MTCD/Publications/PDF/Pub1368_web.pdf

[6] ASTM International, Standard test method for nondestructive assay of special nuclear material in low-density scrap and waste by segmented passive gamma-ray scanning (ASTM Publishing, 2018), https://www.astm.org/c1133_c1133m-10r18.html. Accessed 1 August 2024

[7] ASTM International, Standard guide for making quality nondestructive assay measurements (ASTM Publishing, 2021), https://www.astm.org/c1592_c1592m-21.html. Accessed 1 August 2024

[8] ASTM International, Standard test method for nondestructive assay of radioactive material by tomographic gamma scanning (ASTM Publishing, 2019), https://img.antpedia.com/standard/pdf/F46/1611/ASTM%20C1718-2010_6875.pdf. Accessed 1 August 2024

[9] G.L. Yu, The study of feasibility to detect low signal in gamma-ray spectra using wavelet analysis. Dissertation, Sichuan University, 2005.

[10] R. Venkataraman, M. Villani, S. Croft et al., An integrated tomographic gamma scanning system for non-destructive assay of radioactive waste. Nucl. Instrum. Meth. A. **579**(1), 375–379 (2007). doi: 10.1016/j.nima.2007.04.125

[11] M.M. Hasan, T. Vidmar, J. Rutten et al., Optimization and validation of a $LaBr_3$(Ce) detector model for use in Monte Carlo simulations. Appl. Radiat. Isot. **174**, 109790 (2021). doi:10.1016/j.apradiso.2021.109790

[12] P. Jansson, S. Grape, S. Tobin et al., Comparing HPGe and scintillator detectors for gamma spectroscopy assay of used nuclear fuel (Los Alamos National Laboratory Publishing, 2014), http://www.diva-portal.org/smash/get/diva2:706966/FULLTEXT01.pdf. Accessed 24 Jan 2024

[13] Z.Y. Duan, J.H. Hua, G.X. Zhang et al., Disposal of smooth γ spectrum on Matlab process. Nuclear Power Engineering **28**(3), 125–127 (2007). https://hdlgc.xml-journal.net/article/id/bcf5acbb-6035-4e7e-83cd-62ba067ae34d

[14] H.B. Lu, X. Li, I. Hsiao et al., Analytical noise treatment for low-dose CT projection data by penalized weighted least-square smoothing in the K-L domain. In *Proc. SPIE 4682, Medical Imaging 2002: Physics of Medical Imaging*, vol. 4682, San Diego, California, United States, 3 May 2002. doi:10.1117/12.465552

[15] P. Gorry, General least-squares smoothing and differentiation

by the convolution (Savitzky-Golay) method. Anal. Chem. **62**(6), 570–573 (1990). doi:10.1021/ac00205a007

[16] J. Liu, S.L. Liu, M.E. Meadhat et al., Wavelet transform theory: The mathematical principles of wavelet transform in gamma spectroscopy. Radiat. Phys. Chem. **203**, 110592 (2023). doi:10.1016/j.radphyschem.2022.110592

[17] A.S. Yasin, O.N. Pavlova, A.N. Pavlov, Speech signal filtration using double-density dual-tree complex wavelet transform. Tech. Phys. Lett. **42**(16), 72–78 (2016). doi:10.1134/S1063785016080290

[18] M.I. Hossain, M.A. Rahim, M.N. Hossain, Single-channel speech separation based on double-density dual-tree CWT and SNMF. Ann. Emerg. Technol. Comput. **8**(1), 1–12 (2024). doi:10.33166/AETiC.2024.01.001

[19] L. Zhao, J. Mao, A novel lidar signal denoising method based on variational mode decomposition optimized using whale algorithm. J. Appl. Phys. **135**, 174501 (2024). doi:10.1063/5.0195040

[20] I.H. Elshekhidris, M.B. Mogamedamien, A. Fragoon, Wavelet transforms for EEG signal denoising and decomposition. Int. J. Adv. Signal Image Sci. **9**(2), 11–28 (2023). doi:10.29284/ijasis.9.2.2023.11-28

[21] X.J. Zhang, H.F. Liu, H.S. Zhang, Denoising low activity *gamma*-ray spectra of radon absorbed in activated charcoal by using wavelet thresholding function. Atomic Energy Science and Technology **44**(8), 897-901 (2010). doi:10.7538/yzk.2010.44.08.0897

[22] Y.Y. Luo, L.Q. Ge, C. Xiong et al., Application of wavelet domain Wiener filter in denoising of airborne *gamma*-ray data. Nuclear Techniques **35**(10), 755–758 (2012). https://cstr.cn/32193.14.j.issn.1674-3849.2012.10.755758

[23] D. Vilimek, J. Kubicek, M. Golian et al., Comparative analysis of wavelet transform filtering systems for noise reduction in ultrasound images. PLoS One **17**(7), e0270745 (2022). doi:10.1371/journal.pone.0270745

[24] J. Khalil, S. Kayla, N. Phong et al., Enhancing ECG readability in LVAD patients: A comparative analysis of denoising techniques with an emphasis on discrete wavelet transform. J. Electrocardiol. **85**, 96–108 (2024). doi:10.1016/j.jelectrocard.2024.06.044

[25] Y.C. Yu, L.Q. Ge, F. Li et al., Study on gamma spectrum wavelet noise reduction based on scintillation detector. J. Phys.: Conf. Ser. **1941**, 012027 (2021). doi:10.1088/1742-6596/1941/1/012027

[26] Z. Cui, J.S. Li, Determination algorithm of optimal decomposition level via wavelet entropy. Instrument Technique and Sensor **06**, 127–130 (2015). doi:10.3969/j.issn.1002-1841.2015.06.036

[27] Y. He, X. Zhang, Z. Yao, Improved optimal threshold selection algorithm applied to denoising. Journal of Ordnance Equipment Engineering **40**(3), 127–130 (2015). doi:10.11809/bqzbgcxb2019.03.032

[28] J.H. Liu, X.R. Qin, Y.L. Wang et al., Adaptive denoising of monitoring signal based on dual-tree complex wavelet transform and sample entropy. Journal of Vibration, Measurement & Diagnosis **42**(2), 285–291 (2022). doi:10.16450/j.cnki.issn.1004-6801.2022.02.012

[29] S. Poornachandra, Wavelet-based denoising using subband dependent threshold for ECG signals. Digit. Signal Prog. **18**(1), 49–55 (2008). doi:10.1016/j.dsp.2007.09.006

[30] X. Zhou, Adaptive wavelet thresholding denoising algorithm based on μ law fit. Computer Engineering and Applications **47**(27), 141–143 (2011). doi:10.3778/j.issn.1002-8331.2011.27.038

[31] L.H. Li, J.F. He, Q. Wang et al., Study of γ energy spectrum denoising based on improved wavelet threshold method. Atomic Energy Science and Technology **50**(7), 1279–1283 (2016). doi:10.7538/yzk.2016.50.07.1279

[32] G. Xiao, D. Li, B. Zhang et al., A nonlinear wavelet method for data smoothing of low-level gamma-ray spectra. J. Nucl. Sci. Technol. **41**(1), 73–76 (2004). doi:10.1080/18811248.2004.9715460

[33] Y.C. Yan, M.Z. Liu, F.Z. Liu, Study of smooth processing to gamma energy spectrum by using an average wavelet threshold method. Nuclear Physics Review **31**(3), 407–410 (2014). doi:10.11804/NuclPhysRev.31.03.407

[34] B. Xie, Z.Q. Xiong, Z.J. Wang et al., Gamma spectrum denoising method based on improved wavelet threshold. Nucl. Eng. Technol. **52**(8), 1771–1776 (2020). doi:10.1016/j.net.2020.01.025

[35] S. Meftah, M. Bentoumi, D.H. Burhanuddin et al., Novel leak detector based on DWT an experimental study. Int. J. Robot. Control Syst. **4**(3), 1109–1134 (2024). doi:10.31763/ijrcs.v4i3.1458

[36] X.J. Mou, H.L. Li, X.G. Tu, Research on improved wavelet threshold denoising algorithm and its simulation. Process Automation Instrumentation **41**(8), 46–50 (2020). doi:10.16086/j.cnki.issn1000-0380.2019070036

[37] W. Cao, W. Lu, Y. Shi et al., Dual-attention-based wavelet integrated CNN constrained via stochastic structural similarity for seismic data reconstruction. IEEE Trans. Geosci. Remote Sensing **62**, 1–15 (2024). doi:10.1109/TGRS.2024.3416353

[38] N. Liu, L. Wu, J. Wang et al., Seismic data reconstruction via wavelet-based residual deep learning. IEEE Trans. Geosci. Remote Sensing **60**, 1–13 (2022). doi:10.1109/TGRS.2022.3152984

[39] P. Liu, A. Dong, C. Wang et al., Consecutively missing seismic data reconstruction via wavelet-based Swin residualnetwork. IEEE Trans. Geosci. Remote Sensing **20**, 1–5 (2023). doi:10.1109/LGRS.2023.3265755

[40] D.F. Mix, K. J. Olejniczak, *Elements of Wavelets for Engineers and Scientists* (Wiley, Hoboken, NJ, 2003). doi:10.1063/1.1881903

[41] J.S. Richman, D.E. Lake, J.R. Moorman, Sample entropy. Methods Enzymol. **384**, 172–184 (2004).

[42] P. Heckbert, Fourier transforms and the fast Fourier transform (FFT) algorithm. Comput. Graph. **2**, 15–463 (1995). doi:10.1016/S0076-6879(04)84011-4 https://algoalert.net/pdfs/fourier.pdf

[43] R. Wang, Y.C. Zhang, New threshold function in wavelet threshold de-noising. Computer Engineering and Applications **49**(15), 215–218 (2013). doi:10.3778/j.issn.1002-8331.1211-0364

[44] ORTEC, GammaVision Software User Manual. (AMETEK Inc Publishing, 2020), https://www.ortec-online.com/-/media/ametekortec/manuals/a/a66-mnl.pdf?la=en&revision=dd63bfec-f5cd-4579-8201-e81a52f7fb78. Accessed 20 June 2024

[45] J. Pang (ed.), *Gamma spectrum data analysis* (Shaanxi Science and Technology Press, Xian, 1990).

[46] International Electrotechnical Commission, IEC 61453:2007 (IEC Publishing, 2007)

[47] P. Ormai, A. Fritz, J. Solymosi et al., Inventory determination of low and intermediate level radioactive waste of Paks Nuclear Power Plant origin. J. Radioanal. Nucl. Chem. **211**, 433–451 (1996). doi:10.1007/BF02039710

[48] National Archives: Code of federal regulations (1985), https://www.ecfr.gov/current/title-10/chapter-I/part-61. Accessed 30 January 2024

[49] G.F. Yang, J.C. Dai, X.J. Liu et al., Denoising of gamma-ray spectrum by optimized wavelet thresholding based on modified genetic algorithm in carbon/oxygen logging. J. Radioanal. Nucl. Chem. **320**, 351–359 (2019). doi:10.1007/s10967-019-06477-x

[50] X.Y. Wang, J.F. He, G.M. Wu, Smoothing algorithm of X-ray fluorescence spectrum based on improved wavelet threshold function. Nuclear Electronics & Detection Technology **38**(5), 719–724 (2018). doi:10.3969/j.issn.0258-0934.2018.05.025 , https://webstore.iec.ch/en/publication/5471. Accessed 30 January 2024

[51] Y. Tian, Study on denoising of γ energy spectrum based on mixed noise model. Dissertation, Liaoning Normal University, 2018.